Cardiac magnetic resonance tissue tracking in right ventricle:

Truong, Vien T; Safdar, Komal S; Kalra, Dinesh K; Gao, Xuexin; Ambach, Stephanie; Taylor, Michael D; Moore, Ryan; Taylor, Robin J; Germann, Joshua; Toro-salazar, Olga; Jefferies, John L; Bartone, Cheryl; Raman, Subha V; Ngo, Tam; Mazur, Wojciech

DOI:
10.1016/j.mri.2017.01.007

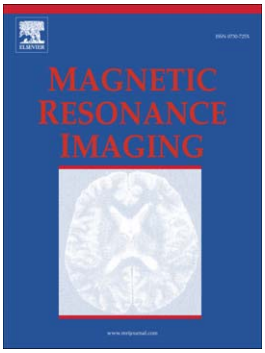

Cardiac magnetic resonance tissue tracking in right ventricle: feasibility and normal values

Vien T Truong, Komal S Safdar, Dinesh K Kalra, Xuexin Gao, Stephanie Ambach, Michael D Taylor, Ryan Moore, Robin J Taylor, Joshua Germann, Olga Toro-Salazar, John L Jefferies, Cheryl Bartone, Subha V Raman, Tam Ngo, Wojciech Mazur

PII: S0730-725X(17)30007-3
DOI: doi:10.1016/j.mri.2017.01.007
Reference: MRI 8714

To appear in: *Magnetic Resonance Imaging*

Received date: 26 March 2016
Revised date: 6 January 2017
Accepted date: 7 January 2017

Please cite this article as: Truong Vien T, Safdar Komal S, Kalra Dinesh K, Gao Xuexin, Ambach Stephanie, Taylor Michael D, Moore Ryan, Taylor Robin J, Germann Joshua, Toro-Salazar Olga, Jefferies John L, Bartone Cheryl, Raman Subha V, Ngo Tam, Mazur Wojciech, Cardiac magnetic resonance tissue tracking in right ventricle: feasibility and normal values, *Magnetic Resonance Imaging* (2017), doi:10.1016/j.mri.2017.01.007

Cardiac magnetic resonance tissue tracking in right ventricle: feasibility and normal values

Vien T Truong MD[1,9*], Komal S Safdar BS[1*], Dinesh K Kalra MD[2], Xuexin Gao[3], Stephanie Ambach[4], Michael D Taylor MD[5], Ryan Moore MD[5], Robin J Taylor MD[6] , Joshua Germann[5], Olga Toro-Salazar MD[7], John L Jefferies MD[5], Cheryl Bartone[1], Subha V Raman MD[8], Tam Ngo MD[9], Wojciech Mazur MD[1]

*These authors contributed equally

(1) The Christ Hospital Health Network, Cincinnati, OH, USA. (2) Rush University medical Center, Chicago, IL, USA. (3) Circle Cardiovascular Imaging Inc, Calgary, Canada. (4) The University of Cincinnati, College of Allied Health Sciences, Cincinnati, OH, USA. (5) Cincinnati Children's Hospital Medical Center, Cincinnati, OH, USA. (6) Centre for Cardiovascular Sciences University of Birmingham, Edgbaston, Birmingham, United Kingdom. (7) Connecticut Children's Medical Center, Hartford, CT, USA. (8) The Ohio State University Medical Center, Columbus, OH, USA. (9) Pham Ngoc Thach University of Medicine, Ho Chi Minh City, Vietnam.

Corresponding Author:
Wojciech Mazur
2139 Auburn Avenue
Cincinnati, Ohio 45219
Phone # 513-721-881
Fax # 513-721-8227
mazurw@ohioheart.org

Acknowledgments: None

Grant Support: None

Running Title: RV Strain Using Tissue Tracking

Abstract

Purpose: To investigate right ventricular (RV) strain in patients without identified cardiac pathology using cardiac magnetic resonance tissue tracking (CMR TT).

Methods:

A total of 50 consecutive patients with no identified cardiac pathology were analyzed. RV longitudinal and circumferential strain was assessed by CMR TT. The age range was 4-81 years with a median of 32 years (interquartile range, 15 to 56 years).

Results

Analysis time per patient was < 5 minutes. The peak longitudinal strain (E_{ll}) was -22.11 ± 3.51%. The peak circumferential strain (E_{cc}) for global, basal, mid-cavity and apical segments were as follows: -11.69 ± 2.25%, -11.00 ± 2.45%, -11.17 ± 3.36%, -12.90 ± 3.34%. There were significant gender differences in peak E_{cc} at the base (P = 0.04) and the mid-cavity (P = 0.03) with greater deformation in females than in males. On Bland-Altman analysis, peak E_{ll} (mean bias, 0.22 ± 1.67; 95% CI -3.05 to 3.49) and mid-cavity E_{cc} (mean bias, 0.036 ± 1.75; 95% CI, -3.39 to 3.47) had the best intra-observer agreement and inter-observer agreement, respectively.

Conclusions: RV longitudinal and circumferential strains can be quickly assessed with good intra-observer and inter-observer variability using TT.

Keywords: Tissue tracking, right ventricular strain, longitudinal strain, circumferential strain, normal values, reproducibility.

Introduction

Recent research demonstrates that for evaluating prognosis in left ventricle (LV) dysfunction, echo derived myocardial strain value can be used as a highly sensitive marker as opposed to the LV ejection fraction (EF), since a reduction in the strain often precedes a decline in EF of patients with LV dysfunction (1,2). Since right ventricular (RV) function is increasingly recognized for its prognostic role in a wide variety of cardiovascular and pulmonary conditions, a lot of effort has been focused on investigating echo derived RV strain, especially longitudinal RV strain (3,4). However, quantitatively evaluating RV function using echocardiography is limited by the complex RV geometry, dense myocardial trabeculations, retrosternal position of the ventricle, and complex motion (5,6). MR imaging can overcome some limitations of echocardiography such as the ability to reproducibly visualize the entire RV. In assessing the RV regional deformation, myocardial tagging is initially applied. However, the laborious post-processing needed to extract and track the tag lines remains the main drawback of basic tagging techniques (2). CMR-derived myocardial feature tracking (FT) is a technique comparable to echocardiography speckle tracking, deriving quantitative deformation parameters from routinely available steady state free precession (SSFP) cine sequences (7), has a relatively short processing time but only measures endocardial strain, with separate analysis needed for epicardial strain (8). On the other hand, CMR-derived myocardial Tissue tracking (TT) uses both endocardial and epicardial borders to determine the myocardial deformable model, then the software constructed a 3D deformable myocardial model based on the tracing, assuming the myocardium is nearly incompressible (9).

Standard steady-state free-precession (SSFP) images are routinely acquired for cardiac functional analysis and it is ideal to obtain strain measurement from such images, since it does

not require additional imaging sequences. In order to measure RV strain and strain from SSFP images and overcome the issues with the existing methods such as relatively long acquisition time and laborious post-processing procedure, we used cardiac magnetic resonance CMR tissue tracking (TT), because this technique can be efficiently implemented in a clinical workflow without extending examination time. The aim of this study was to derive the normal values of RV strain in patients without identified cardiac pathology using CMR TT method.

Materials and Methods

Patient population

A total of 50 consecutive patients with no identified cardiac pathology were retrospectively analyzed. Patients were scanned at The Christ Hospital, Cincinnati Children's Hospital Medical Center in Cincinnati, and Connecticut Children's Medical Center between 2012 and 2015. Only patients with preserved biventricular function (defined as RVEF > 50%, left ventricular ejection fraction (LVEF) > 52% for men and > 54% for women) were included in the analysis. Patients with known conditions affecting RV function such as severe chronic obstructive pulmonary disease (COPD), sleep apnea, morbid obesity, known or suspected pulmonary hypertension, known or suspected shunts were excluded from the study. Patients with significant valvular heart disease identified by echocardiography were excluded as well. This study was approved by the Institutional Review Board.

CMR acquisition

Standard CMR acquisition was performed as reported previously (10). Briefly, imaging was performed on a 1.5 Tesla scanner (Magnetom Avanto, Siemens, Erlangen, Germany), using a phased-array cardiac coil. A horizontal long-axis image and a short-axis RV stack from the atrioventricular ring to the RV apex were acquired using an SSFP pulse sequence (repetition time

of 3.2 ms; echo time of 1.7 ms; flip angle of 60^{o}; sequential 7 mm slices with a 3 mm interslice gap). There were 25 phases per cardiac cycle resulting in a mean temporal resolution of 40 ms.

Tissue Tracking

The RV myocardial deformation was quantified using a prototype of RV specific CVI42 Tissue Tracking software (Circle Cardiovascular Imaging, Calgary, Canada). First, an experienced operator traced the RV endocardial and epicardial borders at the end diastolic (ED) phase in both short-axis and long-axis cine images. The software then constructed a 3D deformable myocardial model based on the tracing, assuming the myocardium is nearly incompressible (9). In each of the subsequent frames the displacements of the myocardial tissues, including the borders, were automatically determined using a gradient-based optical flow method with an incompressible model constraint. The propagated myocardial tissue across the cardiac cycle was verified by the operator to ensure the accuracy of the propagation. Strain values (along the longitudinal, circumferential, and radial directions) for each tissue point as well as the global strain values for the short-axis and long-axis views were automatically derived by the software. The right ventricle was divided into basal, mid-cavity, and apical position to derive regional deformation parameters.

Strain analysis:

The horizontal long axis was used for calculation of longitudinal strain, while the short axis at the base, mid and apex of the right ventricle was used to calculate circumferential strain (figure 1). The interventricular septum was not included in the strain calculation. Endocardial and epicardial contours were drawn in the cardiac phase with the most distinct myocardium boundaries; RV trabeculations were carefully excluded. The software automatically propagated

contours throughout all phases. Longitudinal (E_{ll}) and circumferential strain (E_{cc}) were computed as shown in figure 1.

Reproducibility

Inter-observer variability was assessed in 20 patients using MRI images analyzed by two investigators (K.S and V.T). The same images were analyzed by each operator, who saved the results independently of the other, to provide a blinded assessment. The intra-obsever variability was assessed by investigator 1 (K.S) in 20 patients at two time points 7 -10 days apart.

Statistical analysis

Continuous variables are expressed as mean ± standard deviation (SD) for normal distributions and median + interquartile range for non-normal distributions. Statistical analysis was performed using the SPSS 22 software program. Normality was tested using the Shapiro–Wilk test. Independent sample t-tests were used to compare inter-gender differences. To test for significant differences between RV strain measurements in four patient groups (underweight, normal weight, overweight, obese), analysis of variance (ANOVA) testing was performed. Spearman's Rho correlation test was performed to evaluate the relationships among longitudinal strain and age, and circumferential strain and age. Pearson's correlation coefficient (r) was used to test the association between body mass index (BMI) and strain. Agreement was tested by calculating mean bias and 95% limits of agreement (confidence intervals) from the Bland–Altman analysis, and inter-class correlation coefficient (ICC). A P value of < 0.05 was considered statistically significant.

Results

Patients

This was a retrospective study of 50 consecutive patients without identified cardiac pathology with ages ranging from 4 to 81 years. The median age of patients was 32 years

(interquartile range, 15 to 56 years). There were 22 men with a median age of 32 years (interquartile range, 13 to 58 years) and 28 women with a median age of 32 years (interquartile range, 19 to 52.5 years) (P =0.577). The mean value of RVEF and LVEF were 55 ± 5%; 60 ± 5%, respectively. The LV global longitudinal strain and circumferential strain were -18.15 ± 2.28%; -18.83 ± 2.44% (Table 1).

The average RV longitudinal strain for all 50 patients was -22.11 ± 3.51%. The global RV circumferential strain was -11.69 ± 2.25%. The RV circumferential strain for the basal, mid-cavity, and apical regions were -11.00 ± 2.45%; -11.17 ± 3.36% and -12.90 ± 3.34%, respectively (Table 2). The circumferential strain was higher in the apex than at the base or mid-cavity (P < 0.01 for both) but there was no significant difference between circumferential strain at the base versus the mid-cavity (P= 0.687).

Gender and strain

The peak longitudinal strain (-21.22 vs. -22.80, P=0.11), peak circumferential strain at the apex (-13.36 vs. -12.54, P=0,39), and global circumferential strain (-11.19 vs. -12.09, P=0.15) were similar among males and females. However, there was significant gender difference in peak circumferential strain at the base (-10.20 vs. -11.63, P=0.04) and peak circumferential strain at the mid-cavity (-10.0 vs. -12.09, P=0,03) with greater deformation in females than males (Figure 2).

Age and strain

There was a correlation between peak circumferential strain at the base and age (Spearman's = -0.427, P=0.002). There were no association between longitudinal strain and age (Spearman's = 0.045, P =0.75), global circumferential strain and age (Spearman's = -0.271, P=0.06), peak circumferential strain at the mid-cavity and age (Spearman's =-0.089, P=0.54),

and peak circumferential strain at the apex and age (Spearman's = -0.146, *P* =0.31) (Figure 3). There was significant difference in peak circumferential strain at the base (-9.65 vs -11.70, *P*=0.004), but not in longitudinal strain, mid-cavity and apex in age subgroup analysis (table 3).

BMI and strain

The mean BMI value was 27.77 ± 7.88 kg/m^2. There was no association between BMI and longitudinal strain (r = 0.167, P = 0.26), BMI and global circumferential strain (r = -0.001, P = 0.99), BMI and basal circumferential strain (r =-0.087, P = 0.56), BMI and mid-cavity circumferential strain (r = 0.022, P = 0.88) or BMI and apex circumferential strain (r= 0.041, P = 0.79). There was no significant difference about RV strain between the four patient groups: underweight, normal weight, overweight, obese (p > 0.05 for each).

Reproducibility

Table 2 shows both intra- and inter-observer variability. On Bland-Altman analysis, global peak longitudinal strain (mean bias, 0.22 ± 1.67; 95% CI -3.05 to 3.49) and mid-cavity circumferential strain (mean bias, 0.036 ± 1.75; 95% CI, -3.39 to 3.47) had the best intra-observer agreement and inter-observer agreement, respectively. The circumferential strain at the base and apex had the lowest intra- (0.73 ± 2.21, 95% CI -3.60 to 5.06) and inter- (0.42 ± 1.86, 95% CI -3.23 to 4.07) observer agreement. All parameters had an ICC of ≥ 0.8 (table 4).

DISCUSSION

Transthoracic echocardiography (TTE) derived RV longitudinal strain is assessed reliably from the apical four chamber view, whereas circumferential strain is difficult because it is hampered by a low signal to noise ratio. In contrast, MRI provides highly reproducible information on RV myocardial motion not only in the longitudinal but also in the circumferential direction (5). Tissue Doppler data showed that RV contraction is primarily in the longitudinal

direction (11). However, in conditions leading to RV pressure or volume overload such as pulmonary hypertension, tetralogy of Fallot, or Systemic RV, the contractile pattern changes from longitudinal to circumferential shortening (12-14). As such, it is paramount to define the normal RV strain values derived by CMR TT.

Tagged MRI is the current standard for the assessment of myocardial deformation. There are alternative techniques for measuring RV strain such as the percent segmental shortening (PSS) method (15) and finite element modeling (16). However, all techniques, including myocardial tagging, are very challenging because of a very thin free wall, presence of heavy trabeculations, and resultant laborious post processing (17). While, CMR feature tracking is based on the features at the myocardial boundary voxels and allows tracking with only endocardial or epicardial border defined (10). However, tracking based on the boundary may be subject to errors due to the image noise and the complex anatomical structure along the boundary. In some previous studies using typical feature tracking software, manual corrections were needed for correcting inaccurate tracking results, which could potentially introduce inconsistency into the study (18).

CMR TT requires both endocardial and epicardial borders to determine the myocardial deformable model and it utilizes the nearly incompressible nature of the myocardium during cardiac deformation as an important factor for the tracking equation (9). This additional factor provides information about the myocardium that is not part of the output from the typical feature tracking software. CMR TT allows the tracking to be performed based on the myocardium itself so that its result is not limited to only the features on the boundary voxels and more insensitive to noise. More importantly, typical feature tracking technique for RV strain assessment utilizes a LV tracking program, hence the septal values are included in the analysis, which requires

cumbersome manual editing. The CMR TT software we used in this study provides a dedicated RV strain analysis tool which speeds up our study workflow and also yields more objective results. RV TT method computes the strain with gradient optical flow algorithm which can be very sensitive to morphologic changes affecting RV endocardial or epicardial borders. In our patient population endocardial border correction was required in 20% of patient population likely as result of motion discontinuity. Newer techniques such as variational myocardial myocardial tracking (also performed on cine MRI) is a promising new strain algorhythm designing to properly handle motion discontinuities (19,20).

CMR TT has emerged as a promising method for assessing RV myocardial function. The findings of this study provided normal reference values for RV myocardial strain using CMR TT, derived from 50 patients with no identified cardiac pathology. Kempny et al (21) showed that the value of FT derived RV longitudinal strain and circumferential strain in the short axis view at the level of the papillary muscles in 25 healthy subjects were -24.1 ± 4.0 and -10.6 ± 3.1%, which was concordant with our result. Heermann et al.(22), using FT technique, reported values of RV longitudinal strain and circumferential strain at basal, medial and apical levels in 10 healthy volunteers as −19.3 ± 6, −9.2 ± 3.6, −8 ± 2.8, and −12.5 ± 4.5 respectively. These values are slightly lower than our study. In addition, our results contrasted with those of Youssef et al. who reported mean values for peak circumferential strain of the basal, mid, and apical regions of the RV free wall using strain-encoding MRI as -20.4 ± 2.9%, -18.8 ± 3.9%, and -16.5 ± 5.7%, respectively (23). On the other hand, Ermacora et al. conducted a study in 219 healthy volunteers and reported speckle tracking echocardiography (STE) derived RV longitudinal strain values of -29±4% for the RV free wall and -24±3% for global (3). Preliminary results in patients with history of antracycline exposure (24) , suggest ability of RV TT software to detect subtle

systolic dysfunction when RVEF is still preserved, however robust clinical studies are needed to evaluate this method in wide spectrum of RV pathology affecting not only global but also regional RV function such as ARVC or ischemic heart disease.

This study demonstrated that circumferential strain values were highest at the RV apex. This is consistent with previous echocardiographic data, which found the segmental strain to be significantly higher in the apical segment compared to the basal segment (25,26). Our findings showed that circumferential strain magnitude at the base and mid-cavity were greater in females, with no gender differences noted in apical circumferential and longitudinal strain magnitude. Ermacora et al. found RV longitudinal strain was higher in women than men (-26±3% vs -24±3% for global strain and -32±5% vs -29.2±4.3% for free wall, $p<0.0001$ for both) (3). Moreover, no relationship between age and RV longitudinal strain were found. This is in agreement with the observations of previous investigators using speckle tracking echocardiography (3,26).

This study has some limitations: we did not perform direct comparisons with other techniques such as FT. No comparison was performed with myocardial tagging, SENC or DENSE as those sequences were not available at the time of examination. Our patient population included individuals referred for cardiac MRI rather than healthy volunteers, however we carefully excluded patients with any identified cardiac pathology. In addition, to exclude any possibility of subclinical LV dysfunction we calculated LV global longitudinal and circumferential strain which were in normal range, similar to that reported by Taylor et al (8). Strain measurements are more sensitive to subtle abnormalities of ventricular function than global measures. Despite our attempts to exclude patients with any pathology, which could have affected RV function, some of our subject classified as "normal" on the basis of a lack of global

functional measures, may harbor subtle strain abnormalities. This may be reflected by the wide range of values seen in the scatter plots (Figure 3). Furthermore, given a small number of patients ≥60-65 year old, our results cannot be extrapolated into elderly population as Kawel-Boehm reported significant differences in LV and RV size and function between younger and older adults (27). Lastly, the youngest patient in our population (4 year old) required sedation at the time of CMR examination—we cannot exclude the possibility that this may have possibly affected RV strain .

In conclusion, our data provides evidence that the RV strain can be measured using CMR TT with good intra- and inter-observer reliability, and that it is consistent with the results of other studies (21,28). In addition, the RV strain obtained by using CMR TT with automated software, specifically designed for RV evaluation for strain analysis makes the analysis process time-efficient and practical. Future studies are needed to establish utility of CMR TT in the patients with various RV pathology.

References

1. Poterucha JT, Kutty S, Lindquist RK, Li L, Eidem BW. Changes in Left Ventricular Longitudinal Strain with Anthracycline Chemotherapy in Adolescents Precede Subsequent Decreased Left Ventricular Ejection Fraction. Journal of the American Society of Echocardiography;25(7):733-740.
2. Ibrahim el SH. Myocardial tagging by cardiovascular magnetic resonance: evolution of techniques--pulse sequences, analysis algorithms, and applications. J Cardiovasc Magn Reson 2011;13:36.
3. Ermacora D, Badano LP, Muraru D, et al. Reference values of right ventricular longitudinal strain by speckle tracking echocardiography in 219 healthy volunteers. European Heart Journal 2013;34(suppl 1).
4. Park SJ, Park J-H, Lee HS, et al. Impaired RV Global Longitudinal Strain Is Associated With Poor Long-Term Clinical Outcomes in Patients With Acute Inferior STEMI. JACC: Cardiovascular Imaging 2015;8(2):161-169.
5. Haddad F, Hunt SA, Rosenthal DN, Murphy DJ. Right ventricular function in cardiovascular disease, part I: Anatomy, physiology, aging, and functional assessment of the right ventricle. Circulation 2008;117(11):1436-1448.
6. Ostenfeld E, F AF. Assessment of right ventricular volumes and ejection fraction by echocardiography: from geometric approximations to realistic shapes. Echo Res Pract 2015;2(1):R1-r11.
7. Schuster A, Hor KN, Kowallick JT, Beerbaum P, Kutty S. Cardiovascular Magnetic Resonance Myocardial Feature Tracking. Concepts and Clinical Applications 2016;9(4).

8. Taylor RJ, Moody WE, Umar F, et al. Myocardial strain measurement with feature-tracking cardiovascular magnetic resonance: normal values. European Heart Journal - Cardiovascular Imaging 2015.

9. Bistoquet A, Oshinski J, Skrinjar O. Myocardial deformation recovery from cine MRI using a nearly incompressible biventricular model. Med Image Anal 2008;12(1):69-85.

10. Hor KN, Gottliebson WM, Carson C, et al. Comparison of magnetic resonance feature tracking for strain calculation with harmonic phase imaging analysis. JACC Cardiovasc Imaging 2010;3(2):144-151.

11. Kukulski T, Hubbert L, Arnold M, Wranne B, Hatle L, Sutherland GR. Normal regional right ventricular function and its change with age: a Doppler myocardial imaging study. J Am Soc Echocardiogr 2000;13(3):194-204.

12. Raina A, Vaidya A, Gertz ZM, Susan C, Forfia PR. Marked changes in right ventricular contractile pattern after cardiothoracic surgery: implications for post-surgical assessment of right ventricular function. J Heart Lung Transplant 2013;32(8):777-783.

13. Pettersen E, Helle-Valle T, Edvardsen T, et al. Contraction pattern of the systemic right ventricle shift from longitudinal to circumferential shortening and absent global ventricular torsion. Journal of the American College of Cardiology 2007;49(25):2450-2456.

14. Kind T, Mauritz GJ, Marcus JT, van de Veerdonk M, Westerhof N, Vonk-Noordegraaf A. Right ventricular ejection fraction is better reflected by transverse rather than longitudinal wall motion in pulmonary hypertension. J Cardiovasc Magn Reson 2010;12:35.

15. Klein SS, Graham TP, Jr., Lorenz CH. Noninvasive delineation of normal right ventricular contractile motion with magnetic resonance imaging myocardial tagging. Ann Biomed Eng 1998;26(5):756-763.

16. Haber I, Metaxas DN, Axel L. Three-dimensional motion reconstruction and analysis of the right ventricle using tagged MRI. Med Image Anal 2000;4(4):335-355.

17. Fayad ZA, Ferrari VA, Kraitchman DL, et al. Right ventricular regional function using MR tagging: normals versus chronic pulmonary hypertension. Magn Reson Med 1998;39(1):116-123.

18. Ceelen F, Hunter RJ, Boubertakh R, et al. Effect of atrial fibrillation ablation on myocardial function: insights from cardiac magnetic resonance feature tracking analysis. The International Journal of Cardiovascular Imaging 2013;29(8):1807-1817.

19. Tuyisenge V, Albouy-Kissi A, Sarry L. Variational Myocardial Tracking from Cine-MRI with Non-linear Regularization: Validation of Radial Displacements vs. Tagged-MRI. In: Ourselin S, Rueckert D, Smith N, editors. Functional Imaging and Modeling of the Heart: 7th International Conference, FIMH 2013, London, UK, June 20-22, 2013 Proceedings. Berlin, Heidelberg: Springer Berlin Heidelberg; 2013. p. 334-341.

20. Tuyisenge V, Sarry L, Corpetti T, Innorta-Coupez E, Ouchchane L, Cassagnes L. Estimation of Myocardial Strain and Contraction Phase From Cine MRI Using Variational Data Assimilation. IEEE Trans Med Imaging 2016;35(2):442-455.

21. Kempny A, Fernandez-Jimenez R, Orwat S, et al. Quantification of biventricular myocardial function using cardiac magnetic resonance feature tracking, endocardial border delineation and echocardiographic speckle tracking in patients with repaired

tetralogy of Fallot and healthy controls. Journal of cardiovascular magnetic resonance : official journal of the Society for Cardiovascular Magnetic Resonance 2012;14:32.

22. Heermann P, Hedderich DM, Paul M, et al. Biventricular myocardial strain analysis in patients with arrhythmogenic right ventricular cardiomyopathy (ARVC) using cardiovascular magnetic resonance feature tracking. J Cardiovasc Magn Reson 2014;16:75.

23. Youssef A, Ibrahim el SH, Korosoglou G, Abraham MR, Weiss RG, Osman NF. Strain-encoding cardiovascular magnetic resonance for assessment of right-ventricular regional function. J Cardiovasc Magn Reson 2008;10:33.

24. Truong VT, Safdar KS, Ambach S, et al. Occult Right Ventricular Cardiotoxicity in Childhood Cancer Survivors Undergoing Antracycline Chemotherapy. Journal of Cardiac Failure;22(8):S46.

25. Kowalski M, Kukulski T, Jamal F, et al. Can natural strain and strain rate quantify regional myocardial deformation? A study in healthy subjects. Ultrasound Med Biol 2001;27(8):1087-1097.

26. Levy PT, Sanchez Mejia AA, Machefsky A, Fowler S, Holland MR, Singh GK. Normal ranges of right ventricular systolic and diastolic strain measures in children: a systematic review and meta-analysis. J Am Soc Echocardiogr 2014;27(5):549-560, e543.

27. Kawel-Boehm N, Maceira A, Valsangiacomo-Buechel ER, et al. Normal values for cardiovascular magnetic resonance in adults and children. Journal of Cardiovascular Magnetic Resonance 2015;17(1):29.

28. Morton G, Schuster A, Jogiya R, Kutty S, Beerbaum P, Nagel E. Inter-study reproducibility of cardiovascular magnetic resonance myocardial feature tracking. J Cardiovasc Magn Reson 2012;14:43.

Table 1. Subject Characteristics.

Demographics	Value	Male	Female
Study population	N = 50	N = 22 (44%)	N= 28 (46%)
Median age (IQR) – yr	32 (15-56)	32 (13-58)	32 (19-52.5)
BMI (kg/m2)	27.77 ± 7.88	26.65 ± 7.88	28.6 ± 7.92
RVEF (%)	55 ± 5	56 ± 5	55 ± 4
LVEF (%)	60 ± 5	60 ± 6	60 ± 5
LV global longitudinal strain (%)	-18.15 ± 2.28	-17.39 ± 2.20	-18.75 ± 2.21
LV global circumferential strain (%)	-18.83 ± 2.44	-18.46 ± 1.85	-19.11 ± 2.82

Continuous variable are expressed as mean ± standard deviation with normal distribution and median and interquartile range with non- normal distribution.

IQR, interquartile range; BMI, body mass index; LVEF, left ventricular ejection fraction; RVEF, right ventricular ejection fraction; LV, left ventricular.

Table 2. Right ventricular strain.

RV Strain		Male	Female
Longitudinal strain (%)	-22.11 ± 3.51	-21.22 ± 3.4	-22.8 ± 3.5
	(-21.11 to -23.10)	(-19.71 to -22.73)	(-21.45 to -24.16)
Circumferential strain (%)			
Global	-11.69 ± 2.25	-11.19 ± 1.89	-12.09 ± 2.45
	(-11.05 to -12.33)	(-10.35 to -12.02)	(-11.14 to -13.04)
Basal	-11.00 ± 2.45	-10.2 ± 1.88	-11.63 ± 2.69
	(-10.30 to -11.69)	(-9.34 to -11.03)	(-10.59 to -12.68)
Mid-cavity	-11.17 ± 3.36	-10.00 ± 2.87	-12.09 ± 3.48
	(-10.22 to -12.13)	(-8.73 to -11.27)	(-10.75 to -13.44)
Apex	-12.90 ± 3.34	-13.36 ± 3.57	-12.54 ± 3.17
	(-11.95 to -13.85)	(-11.78 to -14.94)	(-11.32 to -13.77)

Continuous variable are expressed as mean ± standard deviation

RV, Right ventricular

Table 3. Right ventricular strain in age subgoup analysis.

Strain	Age		p
	≤ 18	>18	
Study population (%)	17 (34%)	33 (66%)	
Longitudinal strain (%)	-22.21 ± 3.36	-22.05 ± 3.63	0.88
Circumferential strain (%)			
Global	-10.74 ± 2.17	-12.18 ± 2.15	0.03
Basal	-9.65 ± 1.92	-11.70 ± 2.43	0.004
Mid-cavity	-10.47 ± 3.33	-11.53 ± 3.37	0.29
Apex	-12.09 ± 3.41	-13.32 ± 3.28	0.22

Continuous variable are expressed as mean ± standard deviation

Table 4. Intra-observer and inter-observer variability

Variable (strain)	Variability	Mean bias ± SD	Limits of agreement	P	ICC (95% CI)
Longitudinal	Intra-observer	0.22 ± 1.67	-3.05 to 3.49	0.57	0.87 (0.71-0.95)
	Inter-observer	0.72 ± 1.74	-2.69 to 4.13	0.08	0.85 (0.66-0.94)
Circumferential					
Basal	Intra-observer	0.73 ± 2.21	-3.60 to 5.06	0.15	0.82 (0.60-0.92)
	Inter-observer	-0.45 ± 1.78	-3.94 to 3.04	0.27	0.84 (0.64-0.93)
Mid-cavity	Intra-observer	0.29 ± 1.88	-3.39 to 3.97	0.51	0.88 (0.72-0.95)
	Inter-observer	0.036 ± 1.75	-3.39 to 3.47	0.93	0.91 (0.78-0.96)
Apex	Intra-observer	0.28 ± 1.88	-3.40 to 3.96	0.51	0.83 (0.62-0.93)
	Inter-observer	0.42 ± 1.86	-3.23 to 4.07	0.32	0.83 (0.63-0.93)

Figure 1: CMR tissue-tracking. (A) Longitudinal strain in the four chamber view. (B), (C), (D) Circumferential strain at base, mid-cavity and apex respectively in the short axis view. All images shown are in systole. The yellow color on the images show the tracking of the ventricle. The graphs to the right of each image show the strain value for each of the 25 phases. The peak value was recorded.

Figure 2: Box-and-whisker plot for comparison of RV strain in females and males. Females had greater deformation at the base and mid-cavity levels.

Figure 3: Relationship between age and myocardial strain. R_s represent spearman's rank correlation coefficient. There was a correlation between peak circumferential strain at the base and age.

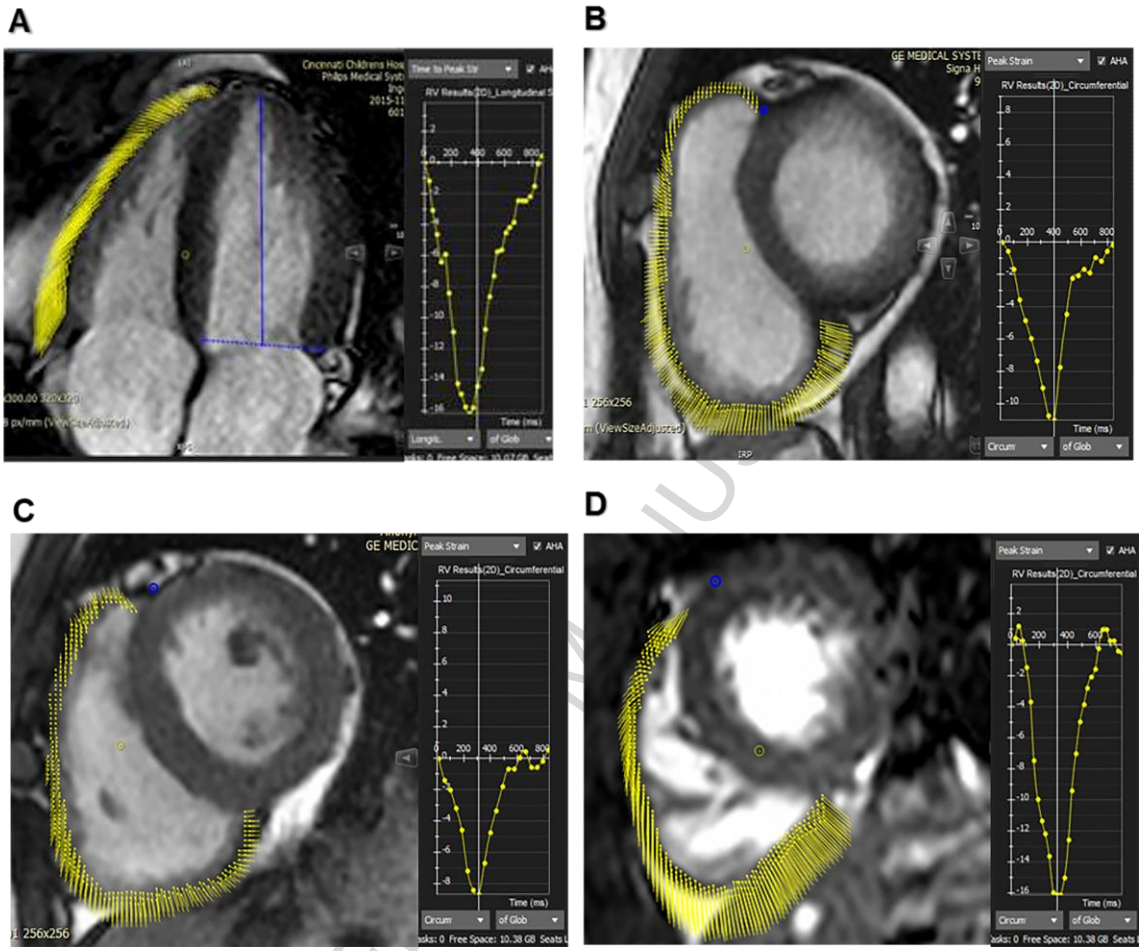

Fig. 1

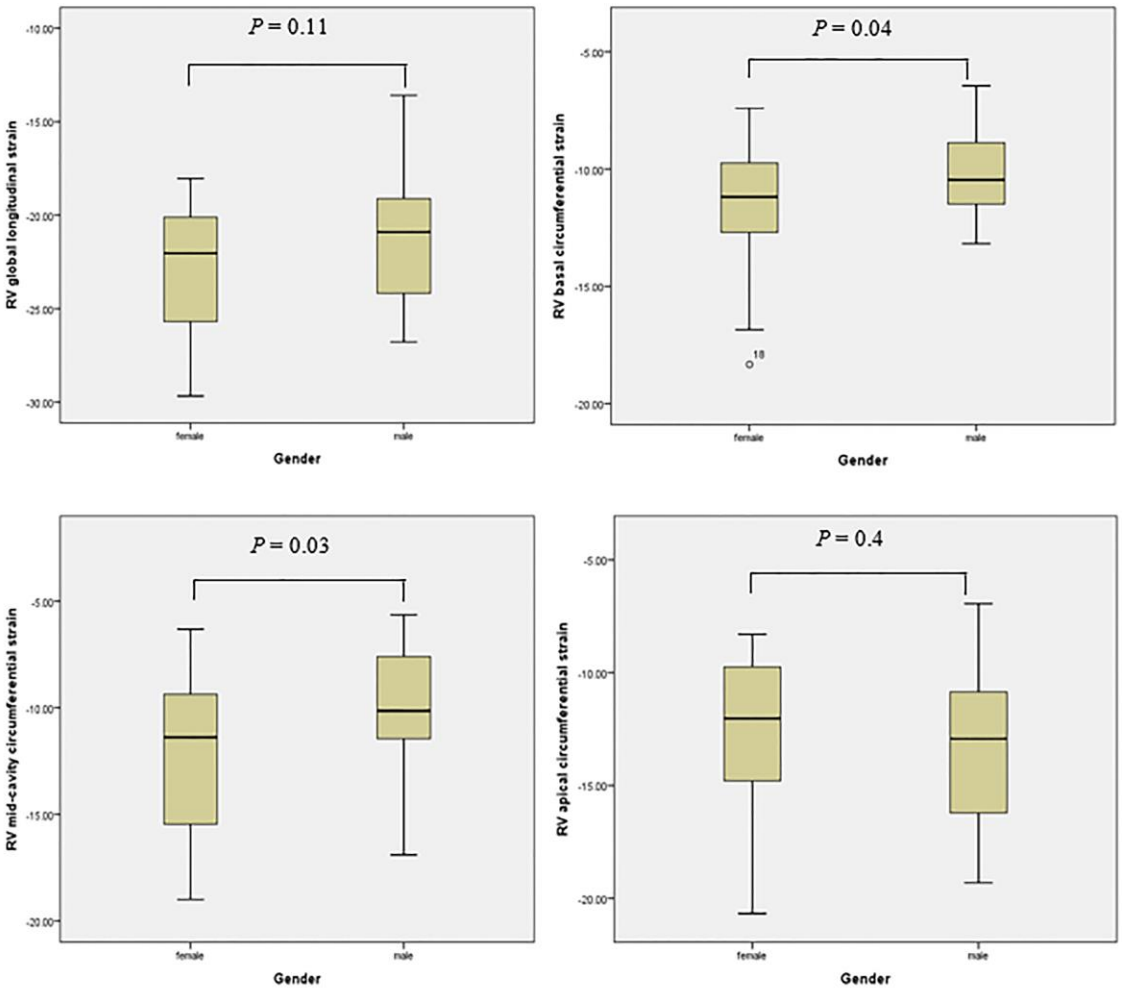

Fig. 2

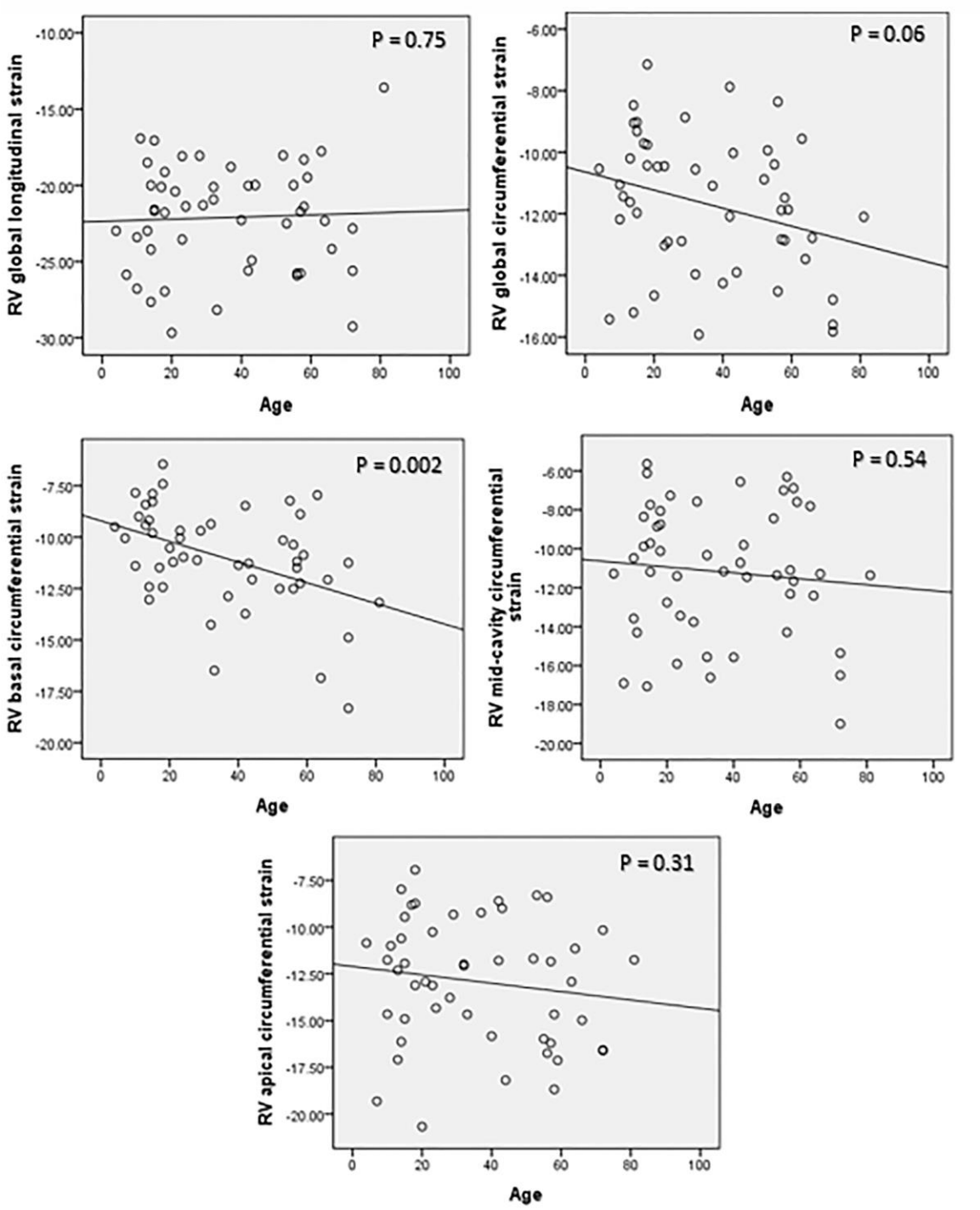

Fig. 3